A Computational Framework for the Simulation of Wind Effects on Buildings in a Cityscape

Donglian Gu[a], Ahsan Kareem[b], Xinzheng Lu[c,*], Qingle Cheng[d]

[a] Research Institute of Urbanization and Urban Safety, School of Civil and Resource Engineering, University of Science and Technology Beijing, Beijing 100083, China

[b] NatHaz Modeling Laboratory, University of Notre Dame, Indiana 46556, USA

[c] Key Laboratory of Civil Engineering Safety and Durability of China Education Ministry, Department of Civil Engineering, Tsinghua University, Beijing 100084, China

[d] School of Civil and Transportation Engineering, Beijing University of Civil Engineering and Architecture, Beijing, 100044, China

[*] Correspondence author: E-mail: luxz@tsinghua.edu.cn

ABSTRACT: Central business districts are densely built with clusters of high-rise buildings that are exposed to winds, impacting their strength, serviceability, and habitability. A computational framework to perform the city-scale evaluation of wind effects on buildings was proposed in this work, while existing studies have been mostly limited to isolated building cases. The framework features (1) a GIS-based topology generation of the cityscape, (2) the large eddy simulation (LES) for time-varying wind loads on buildings, (3) a city-scale time history analysis to capture the building cluster response, (4) a high-fidelity visualization of results, and (5) the city-scale performance assessment. A portion of downtown San Francisco is utilized to demonstrate the framework's potential to usher in a new era in the computational design and assessment of buildings for strength, serviceability, and habitability. The proposed framework offers to complement wind tunnel studies as a virtual twin by enhancing the provision to model building cluster dynamics synchronously. The framework is designed to serve as a system-level computation-based analysis and design platform for building clusters, and does not necessarily aim to reflect recent advances in LES modeling. Each component of the framework is modular and its fidelity can be enhanced by introducing any available refinement.

KEYWORDS: wind-induced building motion; high-rise building; city-scale time history analysis; 3-D dynamic visualization.

1 Introduction

High-rise buildings are important infrastructures in modern cities. The central business districts (CBDs) of some cosmopolitan cities, e.g., Hong Kong and New York, are densely built with clusters of high-rise buildings that experience complex interactions with wind, generating complicated load effects that impact urban planning and their management issues [1, 2].

The design of high-rise building clusters, which is one of the most important aspects of urban planning, faces the challenge of evaluating building performance under winds. In a CBD, the building configuration and its layout can change the wind field, thereby affecting the wind loads and their effects on buildings. Consequently, the design of a specific high-rise building in a CBD-like area warrants attention to the details of the surroundings and it may also have an impact on the performance of surrounding buildings. In the design codes or standards of most countries, while the influence of the surroundings is often included, no information is required to be provided to the existing buildings' management regarding the impact of the new building on the existing buildings. From this perspective, a city-scale assessment method of wind effects on buildings is necessitated to complement the preliminary design of high-rise building clusters. However, existing studies on wind effects on buildings are primarily focused on individual building levels [3-6]. To the best of the authors' knowledge, such holistic city-scale studies have not been done before due to the complexity and challenges involved. This study aims to fill this gap by introducing a novel computational methodology to evaluate building performance under wind effects at a city scale. However, two key challenges must be overcome. One is how to obtain the wind load on each building efficiently in an urban area. The second is

how to obtain an accurate simulation of building responses with computational expediency.

Regarding the first challenge, wind tunnel tests have been widely performed for quantifying wind loads [7-12]. With the advancement of computational fluid dynamics (CFD) and high-performance computing, CFD simulations have been gradually employed [13-18]. Among existing turbulence CFD models, the large eddy simulation (LES) has been recognized to balance the required computing resources and simulation accuracy when the unsteady flow field interacts with buildings resulting in complex aerodynamics [2-4]. Considering that the dynamic response of buildings is required in this context, dynamic wind loads on buildings must be obtained via LES for subsequent dynamic analyses of buildings. However, existing studies that captured wind loads on buildings through LES have been mostly limited to isolated cases [19-22] or with limited surrounding buildings [3, 23, 24]. Even in cases considering surrounding buildings in their CFD simulations, the dynamics of only the target building have been modeled like wind tunnels [3, 23]. In contrast, for high-rise building clusters, mapping flow field data to dynamic wind loads on all buildings at the cityscape is very challenging.

Regarding the second challenge, several methods have been proposed for the wind-induced response simulation of an individual building [25], including the random-vibration-based frequency-domain method [9, 26-30], time history analysis (THA) based on a multiple-degree-of-freedom (MDOF) shear model [31], THA based on a generalized-α model [5], and THA based on a finite element model (FEM) [4, 32, 33]. Table 1 summarizes the computational studies on wind-induced building responses in recent years. Among these studies, the random-vibration-based frequency domain method is the most widely used. However, this method only

offers root mean square values, and determines the peaks using Gaussian assumption, which may limit its application. By contrast, THA can predict the dynamic response at each time step. An initial response to this challenging problem was addressed in our previous study [34].

Table 1. Example of previous computational studies focused on wind-induced building response. CFD: computational fluid dynamics; RANS: Reynolds-averaged Naiver–Stokes equations; LES: large eddy simulation; THA: time history analysis; MDOF: multiple-degree-of-freedom; FEM: finite element model.

Reference	Object of interest	How to capture wind loads on buildings	Turbulence model	How to capture building responses
Li et al., 2003 [31]	An isolated building	Spectral representation method	/	THA based on a MDOF shear model
Swaddiwudhipong & Khan, 2002 [29]	An isolated building	CFD	RANS, LES	Frequency-domain method
Braun & Awruch, 2009 [5]	An isolated building	CFD	LES	THA based on a generalized-α model
Huang et al., 2013 [32]	An isolated building	CFD	LES	THA based on a FEM
Aboshosha et al., 2015 [2]	An isolated building	CFD	LES	Frequency-domain method
Zhang et al., 2015 [4]	An isolated building	CFD	LES	THA based on a FEM
Elshaer et al., 2016 [1]	An isolated building	CFD (surroundings)[a]	LES	Frequency-domain method
Yan & Li, 2016 [3]	An isolated building	CFD (surroundings)	LES	Frequency-domain method
Elshaer et al., 2017 [23]	An isolated building	CFD (surroundings)	LES	Frequency-domain method
Han et al., 2021 [33]	An isolated building	CFD	RANS	THA based on a FEM
Present study	An urban area	CFD	LES	THA based on MDOF shear and flexural–shear models

[a] The CFD simulation considered surroundings.

Targeting the abovementioned challenges, a computational framework for assessing the performance of buildings in winds at a city scale was proposed. A portion of Downtown San Francisco was used as a case study. In the following sections, the proposed framework and

corresponding underlying methodologies are introduced in Section 2, and the case study is presented in Section 3 to showcase the workflow. Section 4 discusses the limitations and future studies. Concluding remarks are given in Section 5.

2 Methodology

The workflow of the proposed framework is outlined in Figure 1. A geographical information system (GIS) was selected as the initial database for this framework. Specifically, seven types of building features, i.e., building polygon, number of stories, structural type, construction year, height, occupancy, and footprint area, are required in the GIS. This is followed by five steps to complete the entire process. Alternative venues (e.g., topology generation schemes [35]) are possible. Additional details are presented in subsequent sections.

(1) Step 1. The CFD model of the target area is constructed based on the building shape information. Subsequently, LES is utilized to obtain the time history data of wind pressures on buildings. (2) Step 2. The wind pressure data is transformed to the time-varying wind loads at building story levels. (3) Step 3. The buildings are modeled as multi-degree-of-freedom (MDOF) shear and flexural–shear models according to their structural characteristics. The city-scale time history analysis (THA) is performed following Step 2 to predict the wind-induced motion of each building concurrently. (4) Step 4. A high-fidelity visualization of the building motion is introduced based on the three-dimensional (3-D) urban model (generated based on the GIS data and Google Earth) and the time history data of building response obtained in Step 3. (5) Step 5. The building response, including occupant comfort of each building, is assessed based on the dynamic building response utilizing a human comfort criterion. The modularity

of the framework permits a user to invoke different comfort criteria they may wish to use. Details of the methodologies for each step are presented in the following sections.

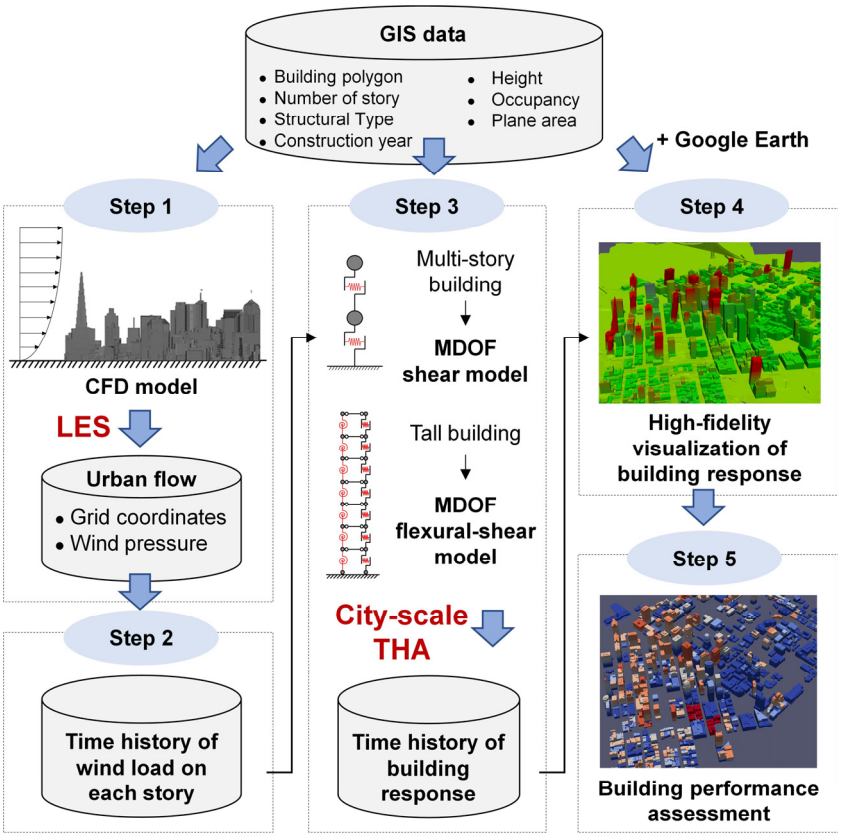

Figure 1. Proposed computational framework. GIS: geographic information system; CFD: computational fluid dynamics; LES: large eddy simulation; MDOF: multiple-degree-of-freedom; THA: time history analysis.

2.1 Flow field simulation for urban area utilizing LES

LES has been used in various urban environment simulations. Table 2 summarizes a sample though not exhaustive of previous typical studies utilizing LES for realistic urban areas. However, these studies mainly focused on the complex urban flow. One step beyond this level of simulation is to simulate the effect of the urban flow on building responses at a city scale. In this study, we performed the LES-based flow field simulation for a part of downtown San Francisco and the subsequent city-scale THA of building cluster response, which to the best of

the authors' knowledge has not been addressed before in any previously reported studies. The details of the simulation will be provided in Section 3.

Table 2. Example of previous typical studies utilizing LES based on a realistic urban area.

Reference	Research topic	Area of interest	Computational domain
Tseng et al., 2006 [36]	Urban flow and pollutant transport	Downtown Baltimore	600 × 600 × 400 m^3
Xie & Castro, 2009 [37]	Flow and dispersion in urban streets	The DAPPLE site in Central London: 800 × 700 m^2	1200 × 800 × 200 m^3
Liu et al., 2011 [38]	Wind field and pollutant dispersion	Downtown Macao: 800 × 800 m^2	1400 × 1100 × 1000 m^3
Letzel et al., 2012 [39]	Pedestrian-level ventilation	Two neighborhoods in Hong Kong	(Lack of description)
Nakayama et al., 2012 [40]	Urban boundary layer flow	A business district in Kyoto: 5000 × 2000 m^2	5000 × 2000 × 1500 m^3
Gousseau et al., 2015 [41]	Near-field pollutant dispersion	Part of downtown Montreal	≈20 m^3 at reduced scale 1:200
Park et al., 2015 [42]	Turbulent flow	An area in Seoul: 3840 × 1290 m^2	7680 × 2400 × 1020 m^3
Yan & Li, 2016 [3]	Wind effects on a super-tall building	Part of central Hong Kong	≈150 m^3 at reduced scale 1:400
Adamek, 2017 [43]	Pedestrian-level wind comfort	The Financial District in Toronto: a circle with a diameter of 610 m	4270 × 2440 × 855 m^3
Jacob & Sagaut, 2018 [44]	Pedestrian-level wind comfort	Shinjuku area in Japan: 1000 × 1000 m^2	4600 × 5000 × 1500 m^3
Kurppa et al., 2018 [45]	Ventilation and air quality	A city boulevard in western Helsinki: 3300 × 54 m^2	4096 × 2048 × 384 m^3
Merlier et al., 2019 [46]	Pollutant dispersion	Part of central Paris	≈50 m^3 at reduced scale 1:350
Auvinen et al., 2020 [47]	Urban boundary layer turbulence	Part of downtown Helsinki: 2200 × 1500 m^2	5120 × 1536 × 400 m^3
Ishihara et al., 2020 [48]	Turbulent flow	The Miyakojima island of Japan	≈50 m^3 at reduced scale 1:1000
Gu et al., 2021 [49]	Wind damage to trees	A university in Beijing: 2000 × 2400 m^2	3585 × 3690 × 507 m^3
Gu et al., 2022 [50]	Wind damage to windows	A community in Shenzhen: 340 × 350 m^2	786 × 834 × 182 m^3
Present study	Wind-induced motion of building cluster	Part of downtown San Francisco: 1950 × 2120 m^2	6400 × 6200 × 1650 m^3

2.2 Time-varying wind load at building story levels

Previous studies have utilized wind-tunnel-based pressure databases [51, 52] for the time history analysis. In the proposed computational framework, the dynamic wind pressure is obtained through the LES scheme. The simulated wind pressure value at each grid point (cell) is a scalar, rather than a vector. The dynamic nature of building motion is simulated using the Cartesian coordinates, requiring the wind pressure normal to the building façade with various shapes be transformed into the wind force in the Cartesian coordinate system of the CFD domain. As an urban area contains a large number of buildings with various shapes, such a wind force transformation must be automated to achieve computational efficiency.

Therefore, a scheme was developed to automatically map the pressure data to wind loads. The workflow of the scheme is shown in Figure 2, which comprises of six steps. In this study, we use the process of determining the wind load on a side (labeled AB) at the second story of the building in Figure 2 as an example:

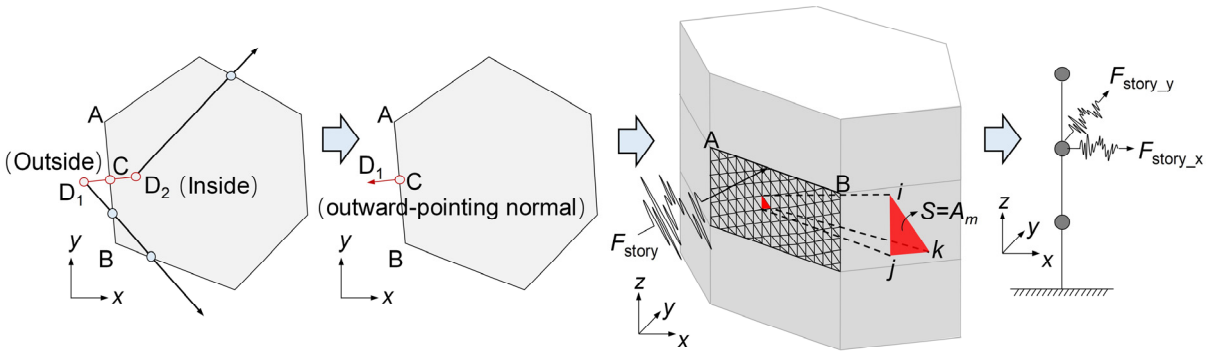

Figure 2. Example of workflow for mapping wind pressure data to dynamic wind load at each story. F_{story}: wind load at the story; F_{story_x}/F_{story_y}: projection of F_{story} on the x/y-axis in the Cartesian coordinate system.

(1) Determine the outward-pointing normal direction of the building polygon:

First, two perpendicular line segments of the length of δ starting from the midpoint

(labeled C) of AB are drawn, generating two endpoints (labeled D_1 and D_2). It is suggested to take a δ less than 0.05 m given that a large value of δ may cause both two endpoints inside the building polygon if the polygon has a concave shape. Subsequently, which point in D_1 and D_2 is outside the building polygon is determined through the even-odd rule. In this example, D_1 is a point outside the polygon. Vector CD_1 is the outward-pointing normal vector of AB in this polygon, which is labeled (p, q) hereinafter.

(2) Compute the wind load acting on the story elevation that contains AB:

All grid points (cells) belonging to the story elevation that contain AB are filtered out. Subsequently, the wind loads on all the selected grids are summed. In this example, the wind load at the second story that contains AB at a specific time step (labeled F_{story} hereinafter) can be calculated using Equations (1) and (2):

$$F_{\text{story}} = \sum_{m=1}^{n} \left(\frac{P_i + P_j + P_k}{3} \cdot A_m \right) \tag{1}$$

$$A_m = \left| \frac{1}{2} \begin{vmatrix} 1 & x_i & y_i \\ 1 & x_j & y_j \\ 1 & x_k & y_k \end{vmatrix} \right| \tag{2}$$

where n is the number of mesh faces of a specific elevation; A_m is the area of the triangle Δ_{ijk}; P_i, P_j, and P_k are the simulated wind pressures on the vertices of the triangle Δ_{ijk}. Generally, if the mesh face has an arbitrary shape with several vertices labeled (x_s, y_s) (s = 1, 2, 3…) clockwise or counterclockwise, F_{story} can be calculated using Equations (3) and (4):

$$F_{\text{story}} = \sum_{m=1}^{n} \left(\frac{\sum_{i=1}^{s} P_i}{s} \cdot A_m \right) \tag{3}$$

$$A_m = \left| \frac{1}{2} \begin{vmatrix} 1 & x_1 & y_1 \\ 1 & x_2 & y_2 \\ 1 & x_3 & y_3 \end{vmatrix} + \frac{1}{2} \begin{vmatrix} 1 & x_1 & y_1 \\ 1 & x_3 & y_3 \\ 1 & x_4 & y_4 \end{vmatrix} + \cdots + \frac{1}{2} \begin{vmatrix} 1 & x_1 & y_1 \\ 1 & x_{s-1} & y_{s-1} \\ 1 & x_s & y_s \end{vmatrix} \right| \tag{4}$$

The projection of F_{story} on the x- and y-axes in the Cartesian coordinate system, $F_{\text{story\_}x}$ and $F_{\text{story\_}y}$, can be calculated using Equations (5) and (6), respectively:

$$F_{\text{story\_}x} = -\frac{F_{\text{story}} p}{\sqrt{p^2 + q^2}} \tag{5}$$

$$F_{\text{story\_}y} = -\frac{F_{\text{story}} q}{\sqrt{p^2 + q^2}} \tag{6}$$

(3) The wind load at the second story of the building at a specific time step can be obtained through summing $F_{\text{story\_}x}$ and $F_{\text{story\_}y}$ on all sides of the story.

(4) The time-varying wind load at the second story can be obtained by repeating steps (1) – (3) for all time steps.

(5) The time-varying wind loads on the specific building can be obtained by repeating steps (1) – (4) for all stories.

(6) The time-varying wind loads on the building cluster can be obtained by repeating steps (1) – (5) for all buildings in the target area.

The above mapping algorithm is developed for buildings without sloped surfaces. By contrast, the area of the mesh face, A_m, should be calculated based on Stokes' theorem for buildings with sloped surfaces. Correspondingly, $F_{\text{story\_}x}$ and $F_{\text{story\_}y}$ can then be calculated using Equations (7) and (8), respectively:

$$F_{\text{story\_}x} = -\frac{F_{\text{story}} p}{\sqrt{p^2 + q^2}} \cos(\theta) \tag{7}$$

$$F_{\text{story}\_y} = -\frac{F_{\text{story}}\, q}{\sqrt{p^2 + q^2}}\cos(\theta) \tag{8}$$

where θ is the angle between the horizontal plane and the normal vector of the sloped surface.

2.3 City-scale time history analysis

An accurate structural dynamics model that can rationally consider the characteristics of different buildings is required to compute the wind-induced vibration of buildings at a city scale. However, for an urban area comprising hundreds of buildings, creating refined computational models is extremely time-demanding. Hence, an efficient modeling method suitable for high-rise buildings and surrounding multistory buildings is desirable. The MDOF models proposed by the authors [53-55] shown in Figure 3 were adopted in this study. Specifically, the MDOF shear model was used to simulate the structure whose deformation mode was dominated by the shear type (e.g., the multistory frame structure), while the MDOF flexural–shear model was adopted for the simulation of the structure with a large height-to-width ratio and a flexural–shear coupling deformation mode (e.g., high-rise frame–shear wall structure). The MDOF shear model assumed that the mass of the structure could be concentrated on the story plane and hence each story could be simplified as a mass point. The mass points between adjacent stories were connected by a shear spring. The trilinear force–deformation model recommended by HAZUS [56] was adopted in the backbone curve of the shear springs. The hysteresis behavior was simulated using a pinching model with only one parameter [54]. By contrast, the MDOF flexural–shear model used both a flexural spring and a shear spring to connect two adjacent stories, so that the flexural–shear coupling deformation mode of high-rise buildings could be captured.

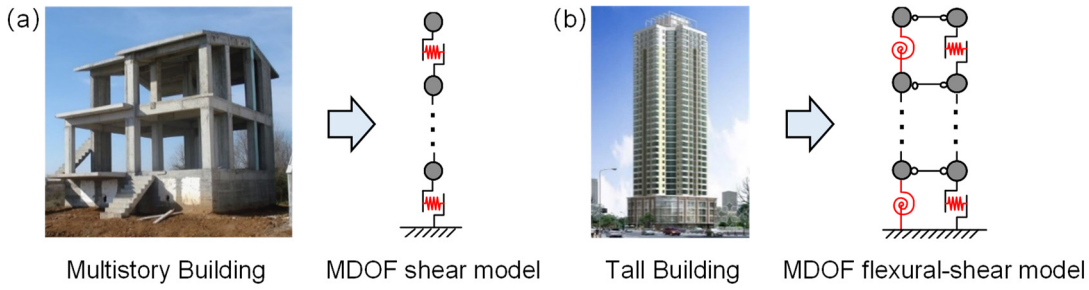

Figure 3. MDOF shear and flexural–shear models.

The parameters of inter-story springs can be determined according to the design drawings. In the absence of design drawings, the authors proposed an automated model generation algorithm to estimate the parameters based on GIS data [54]. Compared to the MDOF shear model adopted by Li et al. [31] and the generalized-α model adopted by Braun & Awruch [5], the abovementioned MDOF models can rationally consider various combinations of the shear deformation and flexural deformation modes in real-world buildings.

The MDOF models have been successfully applied in the regional earthquake simulation [53-55], in which the seismic load of each story was proportional to the acceleration of ground motion. Unlike seismic loads, the dynamic wind loads of stories derived from Section 2.2 need to be directly applied to the mass points of the MDOF models in building response simulations. Hence, we re-coded the city-scale THA algorithm (the original one is open-sourced in the GitHub depository owned by the NHERI SimCenter of the University of California, Berkeley: https://github.com/NHERI-SimCenter/rWHALE/tree/master/Workflow) in this study. Finally, for each building in the target area, the wind-induced dynamic response of each story can be predicted through the central difference scheme. It is worth noting that the MDOF models are not limited to the conditions where the building has an elastic response. They work well even when the structure goes into the inelastic state under some super strong wind events, which

adds to the flexibility of evaluating the building response in the inelastic range needed in some performance-based design scenarios.

2.4 High-fidelity visualization of building response

In this study, the 3-D dynamic visualization method proposed by the authors [57] was adopted to facilitate nonprofessionals (e.g., decision-makers) to better visualize the wind effects on buildings, thus enabling a desirable feature in the performance-based design. The 3-D urban polygonal model constructed based on the GIS data and Google Earth, which provided a realistic urban description, was used as a basis for high-fidelity visualization. The deformations of the MDOF models were mapped to the stories of 3-D polygonal models of buildings, and the deformations of the building polygons between adjacent stories were obtained using the linear interpolation method so that the building objects in the 3-D urban polygonal model could display wind-induced motions.

2.5 Occupant comfort assessment

One of the important building performance measures under winds is the occupant comfort level, which can be assessed for all buildings concurrently at a city scale based on the abovementioned simulation of wind-induced building motions. Several occupant comfort criteria have been studied in the literature [58]. For a certain motion frequency, these criteria provide the perception threshold in terms of peak acceleration. Though it is generally accepted that frequency-dependent peak acceleration is a good indicator of human perception threshold, the root-mean-square (RMS) acceleration that is considered more suitable for evaluating disturbance or annoyance can also be used for occupant comfort assessment [59]. The city-

scale THA method was adopted in this study to predict the wind-induced dynamic response of each building in the computational domain. Consequently, both the peak and RMS values can be obtained easily from the simulation results of time-varying accelerations at any story, without making any assumptions about the probability density function of the acceleration. This feature gives the proposed simulation framework an edge over the frequency domain method. However, it should be noted that for reliable peak estimates, one needs to run longer simulations as done in wind tunnels [60-61]. The corresponding details are available in the following case study.

3 Case Study

A case study for a portion of downtown San Francisco was performed to demonstrate the implementation of the proposed computational framework for regional applications. The study area is the core part of the CBD. It was chosen because the majority of San Francisco's high-rise buildings were included. Specifically, 564 buildings were considered, which encompassed an area of approximately 4 km^2 (Figure 4a). The distribution of building heights is shown in Figure 4b, illustrating that the numbers of buildings higher than 100, 150, and 200 m are 55, 18, and 2, respectively. It is noteworthy that as construction in San Francisco has developed rapidly in recent years, the GIS data obtained in 2017, in this case, may differ from the present. Nevertheless, the case study offers a real-world application of the computational framework to a large cluster of buildings.

3.1 Computational settings

3.1.1 Computational settings of LES

The CFD simulation was carried out under the assumption of neutrally stable atmospheric boundary layer (ABL) conditions without considering thermal effects. As the study case covers an area of approximately 2120 m × 1950 m with a height of H_{max} = 252 m for the tallest building (Figure 4c), a computational domain of 6400 m × 6200 m × 1650 m was constructed (Figure 4d), ensuring an upstream length of 4.5 H_{max}, downstream length of 13 H_{max}, the height of 6.5 H_{max}, and distance of 8 H_{max} from the target area to the lateral boundaries, which complies with the recommendations in COST 732 [17] and AIJ [18] best practice guidelines. Nevertheless, any implementation of this framework would permit an expanded computational domain.

A northwest wind, one of the main wind directions in San Francisco according to historical meteorological data, was selected as an example. At the inflow, the mean speed profile was constructed based on the exposure category of B following ASCE/SEI 7-10 [62], which was given by $U(z) = 33.76\, z^{0.143}$ (U(252 m) = 74.4 m/s, representing a mean recurrence interval (MRI) of 700 years). The Vortex Method was selected to generate the time-dependent wind speed given that this method required neither additional simulation nor extra domain length. The turbulence profile was generated following the Engineering Sciences Data Unit [23]. One could implement a more refined inflow condition using stochastic simulation with divergence-free features available in the NHERI SimCenter tool TinF (https://nheri-simcenter.github.io/TinF-Documentation). The lateral and top boundary conditions were defined as symmetry planes following the best practice guideline [18], and a constant static pressure condition was prescribed at the outlet boundary. The non-slip boundary conditions and standard wall functions were used at the ground and building surfaces. The Wall-Adaptive

Lagrangian-Eulerian model was applied as the sub-grid scale model. Before performing the LES of the case, a 3-D steady-state RANS simulation with the k–ε turbulence model was performed first to install the flow until the wind field reached a relatively steady state so that the computation time for LES could be reduced. The time step of 0.01 s was adopted for the LES. An absolute residual criterion of 1×10^{-4} was used for all parameters. The total simulation time of the LES was 420 s, which corresponds to 4.9 flow-through times ($T_{ft} = L_x/U_h$, where L_x and U_h are the length of the computational domain and the mean speed of the incident flow at the maximum building height). The first 2/3 (280 s) was used for further obtaining a stable urban flow, and the following 1/3 (140 s) was for the wind-induced response analysis of buildings. Parallel computing powered by 640 CPU processers (AMD EPYC 7452 CPU with a clock rate of 2.35 GHz, loaded with the Linux operating system) was used for the CFD computations. Consequently, the computational time for 100 s simulation time was 209 h. Furthermore, a northwest wind scenario with the MRI of 1 year (U(252 m) = 13.5 m/s) was supplemented considering that the 700-year-recurrence wind scenario is generally used for the ultimate design of buildings or safety assessment while the comfort assessment is usually associated with the wind condition with the MRI of 1 year or 10 years. The computational settings of the CFD simulation for the 1-year-recurrence scenario were the same as those used in the 700-year-recurrence scenario.

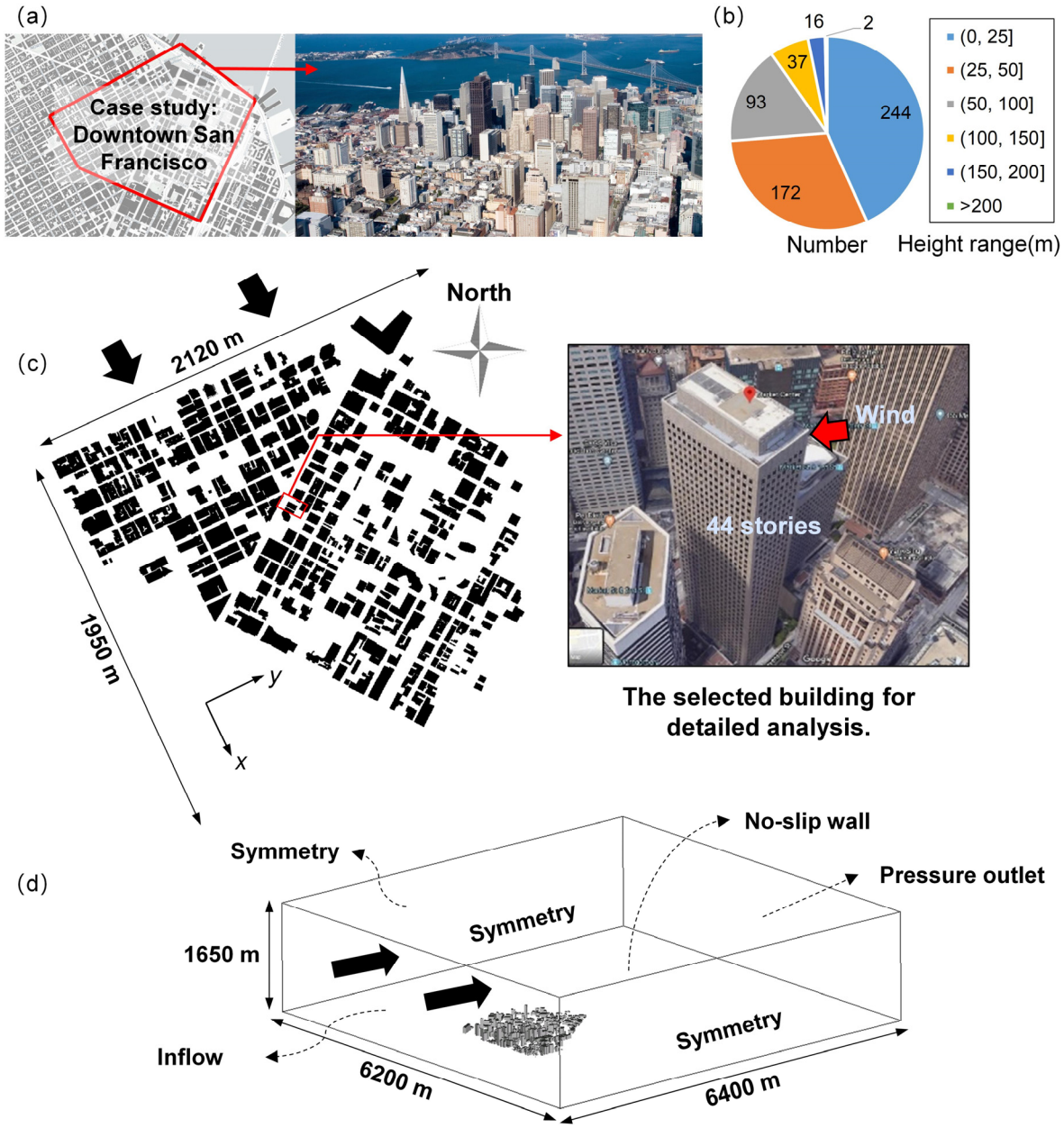

Figure 4. a) A view of downtown San Francisco, b) distribution of building heights, c) the selected building for detailed analysis in the case study, and d) computational domain of the study area.

3.1.2 Computational settings of city-scale THA

With respect to the city-scale THA, the Rayleigh damping with a damping ratio of 1% for all structural modes was adopted [1, 2, 4]. Of course, various damping ratios have been reported on the website http://evovw.ce.nd.edu/damping/dampingdb_noauth1.php developed by the

NatHaz Lab & VORTEX-Winds Group [63]. For example, Jeary proposed an amplitude-related damping ratio for high-rise buildings [64]. More advanced damping models are available in Spence & Kareem [65]. Considering that the damping ratio selected does not affect the proposed framework as a user could select a different value, the damping ratio of all modes of the structure was set as 1% in this case study. The time step of 0.01 s was adopted for the city-scale THA. Consequently, the computational time of the THA for the 700-year-recurrence scenario for all 564 buildings was 3.9 h, while that for the 1-year-recurrence scenario was 3.8 h. Hence, the city-scale THA method is a highly efficient solution to address the second challenge mentioned in Section 1.

3.2 Grid sensitivity analysis of CFD simulation

Although the primary focus of this study is to establish a framework for assessing the wind effects on a cluster of tall buildings, a grid sensitivity analysis of the CFD simulation was conducted so that those adopting this framework should not miss this key step. Three computational grids with different resolutions, namely, fine, basic, and coarse grids, were considered for the grid sensitivity analysis of the CFD simulation based on the 700-year-recurrence scenario.

The fine/basic/coarse gird is composed of three parts, as shown in Figure 5a. (1) Part 1, with a volume of 2000 m × 2200 m × 300 m, contained all buildings in this case and was discretized by the tetrahedral cells. (2) Part 2, which was the domain below 350 m except Part 1, was discretized by the hexahedral cells. (3) Part 3, which was the domain above 350 m, was also discretized by the hexahedral cells. The edge length of the cells in contact with building

walls was smaller than 1 m for the basic grid, while that for the fine and coarse grids did not exceed 0.5 m and 2 m, respectively. The number of cells in the computational domain was 7.08 × 10^8 (fine), 1.77 × 10^8 (basic), and 3.52 × 10^7 (coarse), respectively. Figure 5b shows the grid scheme details and corresponding close-ups of the computational grids.

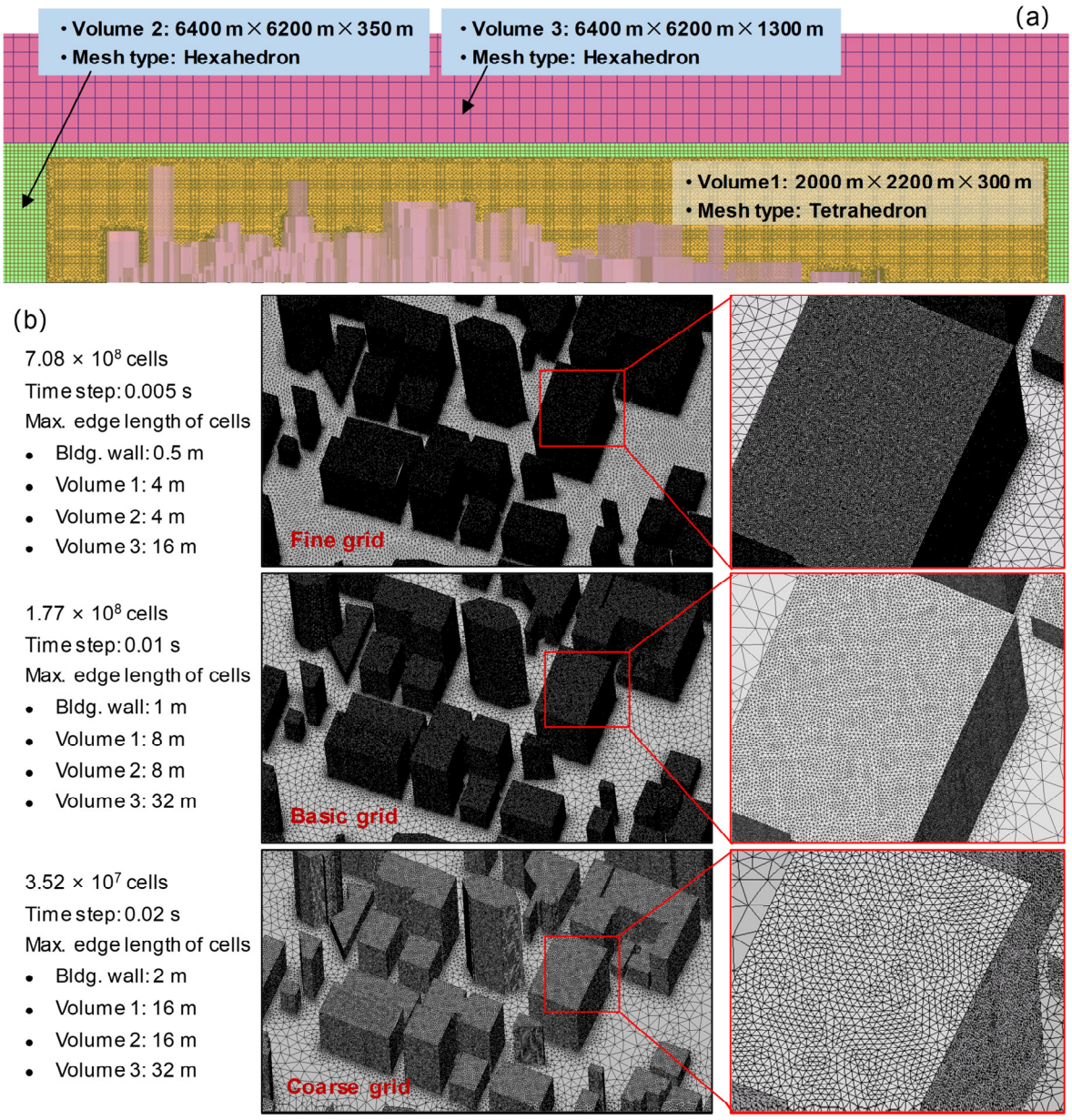

Figure 5. a) Schematic and b) detailed information of grid systems with different resolutions.

Figure 6 shows the grid sensitivity analysis results based on the top-story peak accelerations of all 564 buildings, given that the peak acceleration would be used as the

indicator for occupant comfort assessments in this study (see Section 3.5). All top-story acceleration data were normalized based on the maximum value among the 564 buildings. It can be seen that the normalized top-story acceleration of the basic and fine grids agree well, while the coarse grid cannot generate satisfactory results. Therefore, the basic grid is considered a good tradeoff between accuracy and computational demand. One could invoke additional measures of sensitivity in this exercise.

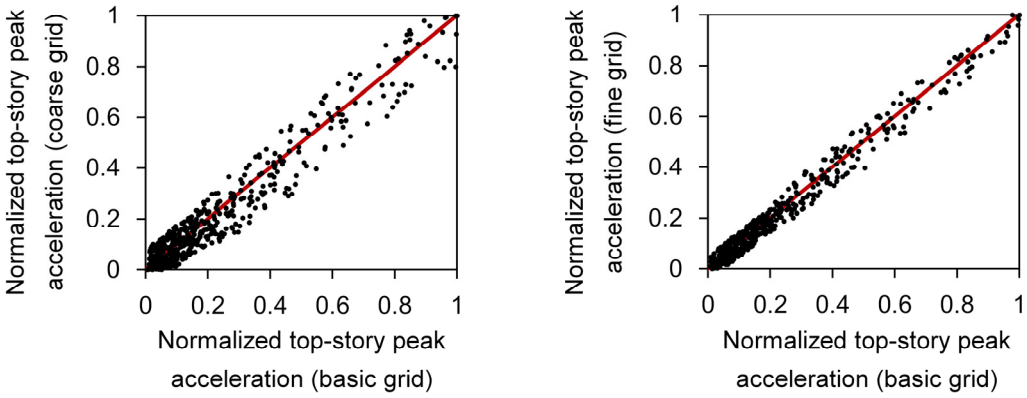

Figure 6. Grid sensitivity analysis results.

3.3 Wind-induced motions of buildings

In this section, the high-fidelity visualization of the wind-induced responses of all 564 buildings is first introduced. Then, a specific high-rise building selected from the buildings taller than 100 m is used to introduce the analysis results in detail. As shown in Figure 4c, the selected 44-story building with a floor area of 1130 m^2 located in the center of the target area exhibits a rectangular-shaped façade (the length and width are 46.5 m and 24.3 m, respectively). The height and regular prismatic form led to the selection of this building.

Furthermore, the simulation results of the 44-story building were compared with wind-tunnel-based aerodynamic databases. A few aerodynamic databases have been established to

facilitate the analysis of the aerodynamic performance of high-rise buildings. For example, the Tokyo Polytechnic University (TPU) aerodynamic database contains wind tunnel test data of wind loads on high-rise building models (http://www.wind.arch.t-kougei.ac.jp/system/eng/contents/code/tpu); the database-enabled design module for high-rise buildings (DEDM-HR, http://evovw.ce.nd.edu/dadm/VW_design6_noauth1.html) developed by the authors provides user-friendly web interfaces for the convenient estimation of wind-induced responses with minimal user input [66]. In this study, the TPU database and DEDM-HR database were utilized to compare the wind pressure and building motion results for the 44-story building, respectively.

3.3.1 Wind-induced motions of all buildings

The high-fidelity visualization of the wind-induced vibrations of the buildings under the 700-year-recurrence wind event is shown in Figure 7 (with a displacement amplification factor of 100), while that in the 1-year-recurrence scenario is shown in Figure 8 (with a displacement amplification factor of 1000). Different colors represent different displacement amplitudes. It should be reemphasized that the 700-year recurrence period is not suitable for human comfort consideration, but was used to observe how the building would perform as the West Coast of the US has recently been battered by hurricane-force winds. It can be seen that, in addition to the buildings, the terrain and bridge were also visualized in the urban scene. An animation of the building motions under the 700-year-recurrence scenario can be viewed directly at https://cloud.tsinghua.edu.cn/f/46f57e68c6584f24bca1, which can provide more intuitive information to facilitate the decision-making of nontechnical people, especially for the

performance-based design.

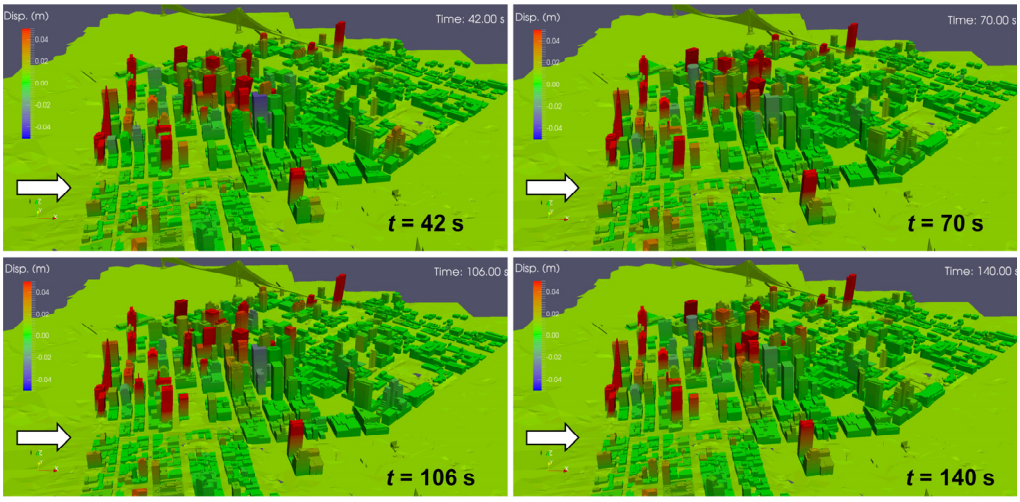

Figure 7. Visualization of wind-induced building vibrations under the 700-year-recurrence scenario (displacement amplification factor: 100).

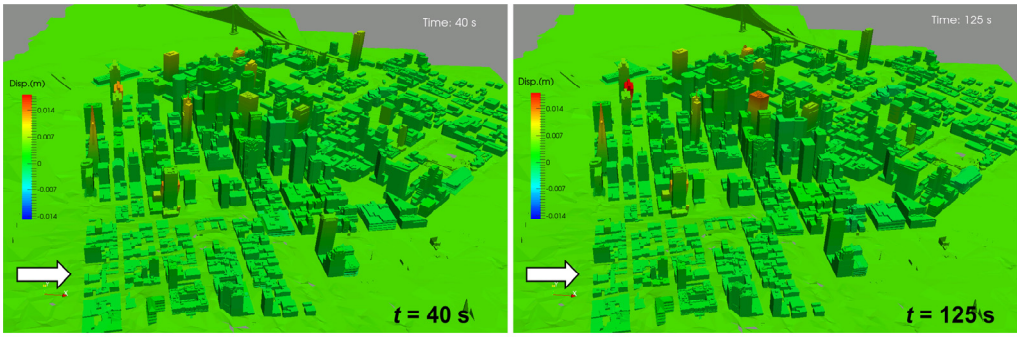

Figure 8. Visualization of wind-induced building vibrations under the 1-year-recurrence scenario (displacement amplification factor: 1000).

3.3.2 Wind-induced motion of the 44-story building

(1) Wind pressure coefficients C_p

Most of the neighboring high-rise buildings are lower than this typical 44-story building. Figure 9 shows the mean, RMS, and peak C_p distributions across a horizontal section at 2/3 of the building height under the attack angle of 37.4°. The positive mean C_p occurs on the northwest and northeast sides of this building, given that the neighboring buildings are not high enough to bring a significant shadow effect on these two windward sides. By contrast, the mean C_p on the leeward sides of the building is negative. The RMS C_p is in the range of 0.02 to 0.32.

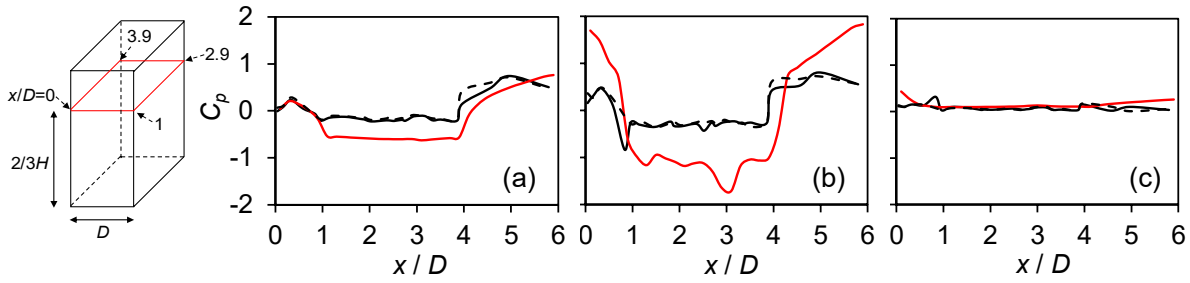

Figure 9. a) Mean, b) peak, and c) RMS C_p distributions over a horizontal section. The black lines represent the case study results under the 700-year-recurrence (solid line) and 1-year-recurrence (dotted line) scenarios, while the red lines indicate the TPU database results.

The TPU database was utilized to compare the wind pressure results. Figure 9 shows the comparison results for the mean, peak, and RMS C_p. It can be seen that the trend of the mean and peak C_p distributions is consistent with those obtained from the TPU database. However, the mean C_p obtained through the TPU database on the leeward surface ($1 < x/D < 3.9$) is larger than that of the San Francisco case, in part due to the presence of surrounding buildings whereas the database comprises of isolated building cases. The peak C_p obtained through the TPU database at most sample points is accordingly larger than that of the San Francisco case. Likely, the aerodynamics of an isolated building (as the case in database measurements) experiences larger excursions of pressure, while the excursions are dampened when a building is immersed in surroundings, as noted in studies dealing with the influence of turbulence. Once again, it should be noted that the primary focus of this study was to establish a holistic framework for assessing building performance such as displacements and accelerations, rather than introduce the advances in the LES simulation quality that have been studied in numerous papers in the literature. One can use a more refined CFD computational domain and compare it to a site-specific wind tunnel study to further enhance the efficacy of the virtual computational platform.

(2) Displacement and acceleration responses

In this section, the building response results of the 44-story building are discussed. Figure 10a shows the trajectory of the top story. It can be observed that the building vibrates along the north-south direction given the influence of the surrounding buildings in the cluster. As shown in Figure 10b, the profile of the peak displacement demonstrates that the typical 44-story building has an obvious flexural–shear coupled deformation mode, which is difficult to simulate through the structural models used by studies listed in Table 1. Figure 10c shows the acceleration fluctuation at the top story. The peak accelerations in the *x*- and *y*-directions under the 700-year-recurrence scenario are 0.11 m/s^2 (11.22 mg) and 0.13 m/s^2 (13.27 mg), respectively, while those under the 1-year-recurrence scenario are 1.15 mm/s^2 (0.12 mg) and 1.24 mm/s^2 (0.13 mg), respectively. The phase of fluctuations in the acceleration time histories in the *x*- and *y*-directions reflects the nature of the trajectory of the top story in Figure 10a. This may be introduced by the complexity of flow in the urban canyon. For the strength design under 700-year winds, the base bending moments and base sheers can be easily obtained using the MDOF models of buildings though they are not presented here for brevity.

The DEDM-HR database was utilized to compare the building motion results. The comparisons between the DEDM-HR-based predictions and the simulated San Francisco case are given in Table 3. For the 700-year-recurrence scenario, the peak displacement and peak acceleration results of the San Francisco case in the depth direction agree well with the DEDM-HR results. For the RMS acceleration in the breadth direction, the San Francisco case is also in good agreement with the DEDM-HR results. However, for the peak displacement and peak acceleration in the breadth direction, the relative differences reach -24.53% and -22.61%,

respectively. In balance, the mean relative differences in two directions for the peak displacement, peak acceleration, and RMS acceleration are -3.06%, -13.47%, and 11.75%, respectively. For the 1-year-recurrence scenario, the San Francisco case agrees well with the DEDM-HR results in terms of the peak displacements and depth-direction RMS acceleration. The relative differences concerning the peak accelerations and breadth-direction RMS acceleration are large. Considering that building response amplitudes under the 1-year-occurrence wind are very small, the abovementioned relative difference is plausible due to noise and uncertainty at low amplitude oscillations resulting from low intensity of loading.

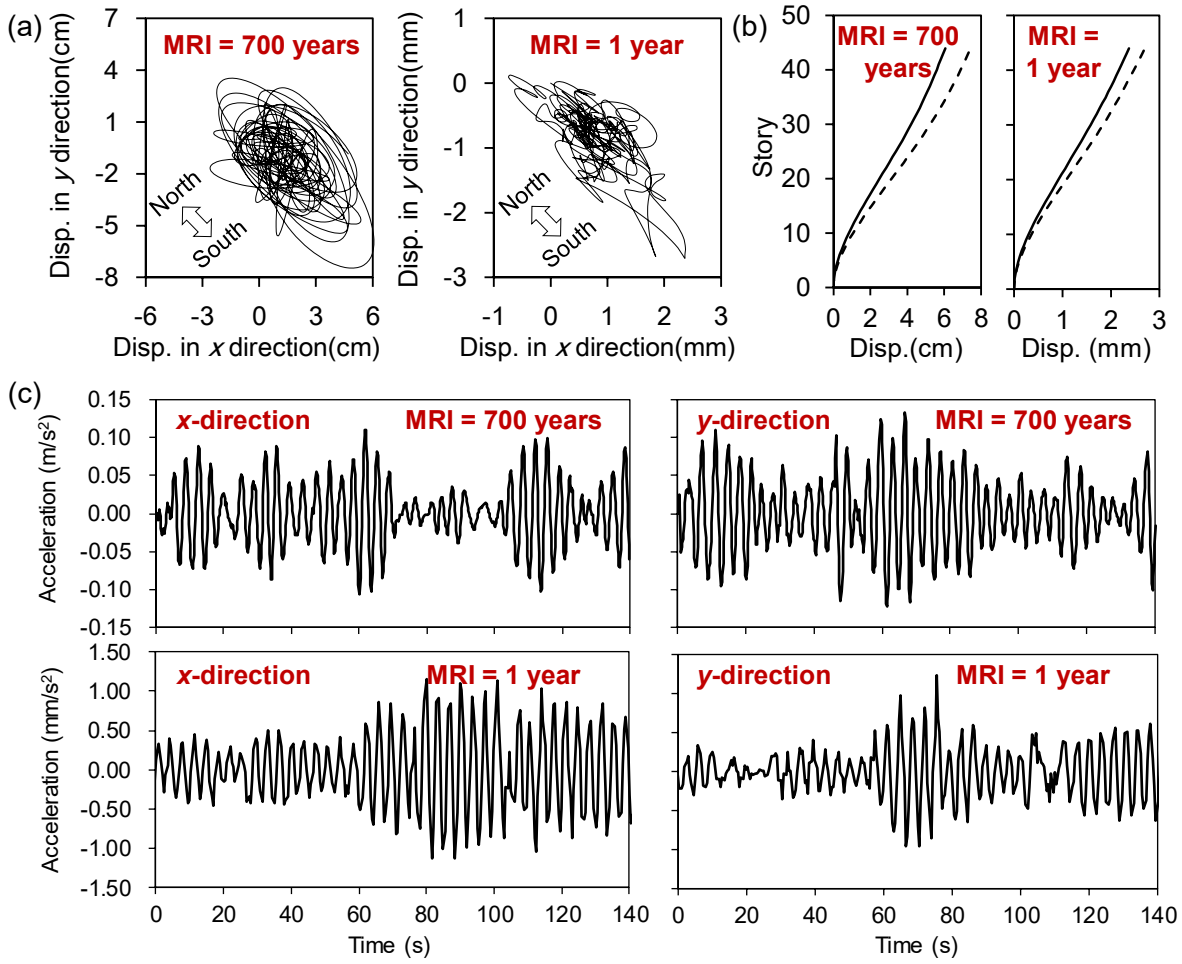

Figure 10. a) Trajectories, b) peak displacement profiles (*x*-direction: solid line; *y*-direction: dotted line), and acceleration fluctuations of the top story.

Table 3. Comparison between the DEDM-HR results and SF downtown case results.

MRI = 700 years	**Building response at roof in the depth direction**		
	Peak displacement	Peak acceleration	RMS acceleration
San Francisco case	0.090 m	0.155 m/s^2	0.053 m/s^2
DEDM-HR	0.076 m	0.162 m/s^2	0.042 m/s^2
Relative difference	18.42%	-4.32%	26.19%
MRI = 700 years	**Building response at roof in the breadth direction**		
	Peak displacement	Peak acceleration	RMS acceleration
San Francisco case	0.040 m	0.089 m/s^2	0.036 m/s^2
DEDM-HR	0.053 m	0.115 m/s^2	0.037 m/s^2
Relative difference	-24.53%	-22.61%	-2.70%
Mean relative difference of two directions	-3.06%	-13.47%	11.75%
MRI = 1 year	**Building response at roof in the depth direction**		
	Peak displacement	Peak acceleration	RMS acceleration
San Francisco case	0.0036 m	0.0039 m/s^2	0.0015 m/s^2
DEDM-HR	0.0036 m	0.0056 m/s^2	0.0014 m/s^2
Relative difference	0	-30.36%	7.14%
MRI = 1 year	**Building response at roof in the breadth direction**		
	Peak displacement	Peak acceleration	RMS acceleration
San Francisco case	0.0011 m	0.0021 m/s^2	0.0008 m/s^2
DEDM-HR	0.0012 m	0.0034 m/s^2	0.0010 m/s^2
Relative difference	-8.33%	-38.24%	-20.00%
Mean relative difference of two directions	-4.17%	-34.30%	-6.43%

Also, estimates of the peak value of the response from simulated data have larger uncertainty due to the short length of the data and the method of estimation, whereas the values from the DEDM-HR database are based on a Gaussian assumption using a peak factor approach. Regardless, these results are very encouragingly close in light of the major difference between simulation conditions and measurements in the database values, i.e., an isolated building case versus a building in a large cluster. More refined grids and longer records used in estimating peaks by fitting probability density functions or averaging the peaks of segments/ensembles

may aid in closing this gap.

3.4 Occupant comfort assessments

One of the important building performance measures under winds is the occupant comfort level. The occupant comfort criterion recommended by AIJ-GEH-2004 criterion [67] was used here for the occupant comfort assessment, given that it is aimed at performance-based wind design. AIJ-GEH-2004 uses the peak acceleration to evaluate occupant comfort and categorizes the comfort quality into five levels: H-10, H-30, H-50, H-70, and H-90, which represent 10%, 30%, 50%, 70%, and 90% of the persons in the building who can feel the wind-induced vibration, respectively. Although this criterion recommends applying the 1-year-recurrence peak acceleration for habitability evaluation, users can evaluate the occupant comfort through the evaluation curves for hazard scenarios with any return period given that the evaluation curves issued by AIJ-GEH-2004 were obtained by the shaking table tests independent of the hazard return period. By contrast, the allowable levels or design guidelines for occupant comfort are deterministically specified in other frequency-related criteria like ISO 10137-2007 [68] for wind scenarios with the MRI of 1 year or 10 years.

The assessment results of all 564 buildings in the downtown San Francisco case are shown in Figure 11. Under the 700-year-recurrence wind, among the 55 buildings over 100 m, 87.3% of the buildings indicate an occupant comfort quality of H-90 on the top story. Hence, the northwest wind scenario with the MRI of 700 years is worth paying attention to for downtown San Francisco considering that the high-rise buildings accommodate a large number of people in the city. An assessment at this level of winds is currently not needed in design but was

introduced to see how many buildings will be influenced when unusual winds are experienced, which is a question asked out of curiosity by stakeholders sometimes. By contrast, under the 1-year-recurrence wind, there are only two buildings whose occupant comfort qualities of the top story reach H-50, indicating that this wind scenario is considered to have a slight effect on the building function. Furthermore, it can be observed from Figure 11 that the occupant comfort quality of each story can be visualized with high fidelity through the proposed framework.

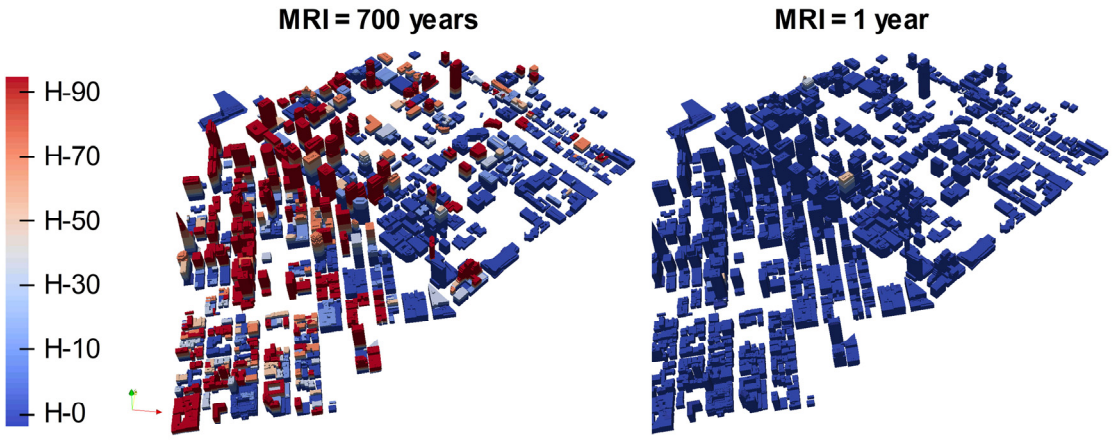

Figure 11. Visualization of occupant comfort levels for all 564 buildings.

The results of pedestrian-level winds are not included here for brevity given that they can be obtained without any additional effort. In fact, winds at each cell level are available in the entire domain which facilitates visualizing the flow field at any level as it passes by the cluster of buildings.

4 Limitations and future studies

The proposed method necessitates a significant amount of storage space to store time-varying urban flow and building cluster response data. More than 20 terabytes of storage space was specifically used to store the simulation results for the case study. As a result, given the

computing resources, time costs, and storage space, the sampling period of CFD simulations in this example may be on the lower side at this point. Nonetheless, the sampling period in the example has no influence on the demonstration of the effectiveness of the proposed computational framework. Future studies, once additional resources become readily available, will include a simulation with a longer sampling period and emphasis on refining the computational scheme within the framework.

Furthermore, it is noteworthy that the fluid–structure interaction was not considered since the structural stiffness of most high-rise buildings is sufficient to resist the excessive motion that would warrant invoking non-negligible effects on wind fields. Nevertheless, based on this study, the fluid–structure interaction can be implemented conveniently through computational schemes that involve fully-coupled fluid and structure domains at different levels of sophistication. This study is an initial system-level effort to advance this proposed framework in the hope that the increasing availability of computational resources in the cloud environment will make it a viable platform that could be used in a whole-city-scale simulation with additional desired refinements of the computational domain.

5 Concluding Remarks

In the prevailing digital world, the planning, management, and design of cities face the challenge of computationally simulating the wind effects on buildings situated in urban clusters and the corresponding assessment of strength requirements and habitability at the city scale. In this study, a computational framework for the assessment of wind effects on buildings at a city scale using the GIS, LES, and THA is proposed. The main features are highlighted as follows:

(1) The proposed framework enables the assessment of the collective building performance at various scales, i.e., city scale, individual building scale, and story level scale. The modularity of the framework permits enhancing the level of sophistication for each component module for assessing the desired prescribed metrics required in the performance-based design, e.g., strength, serviceability, human comfort and plaza level winds.

(2) The framework offers a high-fidelity display of wind-induced building motions and to what extent the motion level leads to meeting or exceeding the performance metrics. Such visualizations can facilitate lay stakeholders a better understanding of the simulated scenarios.

(3) A case study of a part of downtown San Francisco was performed, indicating the efficacy of the framework and ushering in its potential application as a system-level computation-based design and planning approach for resilient cities.

(4) The simulated wind pressures on buildings and corresponding building responses were compared to the wind-tunnel-based pressure database and database-enabled response predictions, respectively.

(5) The framework has a promise to usher in a new era in the computational design and assessment of buildings for strength and serviceability. It can be further enhanced by the inclusion of more advanced inflow features, more refined LES simulations, and the provision of aeroelastic effects.

Acknowledgements

First of all, we would like to recognize the opportunity that Prof. Shuzo Murakami offered to the second author in the early 1990s by hosting a visit to the University of Tokyo as a visiting

professor and later invitation to join the historic first conference on Computational Wind Engineering (CWE). The second author was introduced to their work at the University of Tokyo and had the opportunity to interact with Profs. A. Mochida and Y. Tominaga. This led to the second author's first paper on the CFD presented at the first CWE Conference in 1992 in Tokyo and later published in the Volume 46 and 47 in the Journal of Wind Engineering & Industrial Aerodynamics in 1993. It was followed by several papers on LES simulation of flow and pressure fields around prisms of various aspect ratios in the Journal of Wind Engineering & Industrial Aerodynamics and a forthcoming paper in the Journal of Fluid Mechanics. Once again, we are thankful to Prof. Murakami for hosting the second author's visit in the 1990s which led to these developments. We also thank Profs. Y. Tominaga and T. Stathopoulos for their kind invitation to this special issue celebrating the first Conference on CWE in 1992.

This work was supported by the National Natural Science Foundation of China (No. 52208456, 52238011), the SimCenter under NSF grant CMMI 2131111, and the Tencent Foundation through the XPLORER PRIZE. The authors appreciate Beijing Computing Center for providing the computational hardware and software that were used in this work.

References

[1] Elshaer, A., Aboshosha, H., Bitsuamlak, G., El Damatty, A., & Dagnew, A. (2016). LES evaluation of wind-induced responses for an isolated and a surrounded tall building. Engineering Structures, 115, 179−195. http://dx.doi.org/10.1016/j.engstruct.2016.02.026

[2] Aboshosha, H., Elshaer, A., Bitsuamlak, G. T., & El Damatty, A. (2015). Consistent inflow turbulence generator for LES evaluation of wind-induced responses for tall buildings.

Journal of Wind Engineering and Industrial Aerodynamics, 142, 198−216. http://dx.doi.org/10.1016/j.jweia.2015.04.004

[3] Yan, B. W., & Li, Q. S. (2016). Large-eddy simulation of wind effects on a super-tall building in urban environment conditions. Structure and Infrastructure Engineering, 12(6), 765-785. https://doi.org/10.1080/15732479.2015.1051997

[4] Zhang, Y., Habashi, W. G., & Khurram, R. A. (2015). Predicting wind-induced vibrations of high-rise buildings using unsteady CFD and modal analysis. Journal of Wind Engineering and Industrial Aerodynamics, 136, 165−179. https://doi.org/10.1016/j.jweia.2014.11.008

[5] Braun, A. L., & Awruch, A. M. (2009). Aerodynamic and aeroelastic analyses on the CAARC standard tall building model using numerical simulation. Computers & Structures, 87(9−10), 564−581. https://doi.org/10.1016/j.compstruc.2009.02.002

[6] Tamura, T., Nozawa, K., & Kondo, K. (2008). AIJ guide for numerical prediction of wind loads on buildings. Journal of Wind Engineering and Industrial Aerodynamics, 96(10-11), 1974-1984. https://doi.org/10.1016/j.jweia.2008.02.020

[7] Li, Q. S., Wu, J. R., Liang, S. G., Xiao, Y. Q., & Wong, C. K. (2004). Full-scale measurements and numerical evaluation of wind-induced vibration of a 63-story reinforced concrete tall building. Engineering Structures, 26(12), 1779−1794. https://doi.org/10.1016/j.engstruct.2004.06.014

[8] Kareem, A., & Cermak, J. E. (1979). Wind tunnel simulation of wind-structure interactions. ISA Transactions, 18(4), 23–41.

[9] Kareem, A. (1982). Fluctuating wind loads on buildings. Journal of the Engineering Mechanics Division, 108(6), 1086-1102. https://doi.org/10.1061/JMCEA3.0002892

[10] Kareem, A. (1982). Acrosswind response of buildings. Journal of the Structural Division, 108(4), 869-887. https://doi.org/10.1061/JSDEAG.0005930

[11] Li, X., & Li, Q. S. (2021). Monitoring of wind effects on a super-tall building during multiple typhoons and validation of wind tunnel testing techniques. Structure and Infrastructure Engineering, 17(11), 1535-1551. https://doi.org/10.1080/15732479.2020.1815806

[12] Li, X., Yu, X., Li, Q. S., & Allsop, A. (2021). Field measurement and validation of structural dynamic parameters of skyscrapers under super typhoon excitation. Journal of Civil Structural Health Monitoring, 11(3), 609-627. https://doi.org/10.1007/s13349-021-00470-3

[13] Dagnew, A. K., & Bitsuamlak, G. T. (2014). Computational evaluation of wind loads on a standard tall building using LES. Wind and Structures, 18(5), 567−598. https://doi.org/10.12989/was.2014.18.5.567

[14] Zhang, A., & Gu, M. (2008). Wind tunnel tests and numerical simulations of wind pressures on buildings in staggered arrangement. Journal of Wind Engineering and Industrial Aerodynamics, 96(10−11), 2067−2079. https://doi.org/10.1016/j.jweia.2008.02.013

[15] Kareem, A., Bernardini, E., & Spence, S. M. (2013). Control of the wind induced response of structures. Advanced Structural Wind Engineering, 377-410.

https://doi.org/10.1007/978-4-431-54337-4_14

[16] Kareem, A. (2020). Emerging frontiers in wind engineering: Computing, stochastics, machine learning and beyond. Journal of Wind Engineering and Industrial Aerodynamics, 206, 104320. https://doi.org/10.1016/j.jweia.2020.104320

[17] Franke, J., Hellsten, A., Schlünzen, H., & Carissimo, B. (2007). Best Practice Guideline for the CFD Simulation of Flows in the Urban Environment, Cost Action 732: Quality Assurance and Improvement of Microscale Meteorological Models. COST office, Brussels.

[18] Tominaga, Y., Mochida, A., Yoshie, R., Kataoka, H., Nozu, T., Yoshikawa, M., & Shirasawa, T. (2008). AIJ guidelines for practical applications of CFD to pedestrian wind environment around buildings. Journal of Wind Engineering and Industrial Aerodynamics, 96(10-11), 1749−1761. https://doi.org/10.1016/j.jweia.2008.02.058

[19] Ricci, M., Patruno, L., & De Miranda, S. (2017). Wind loads and structural response: benchmarking LES on a low-rise building. Engineering Structures, 144, 26−42. http://dx.doi.org/10.1016/j.engstruct.2017.04.027

[20] Ricci, M., Patruno, L., Kalkman, I., De Miranda, S., & Blocken, B. (2018). Towards LES as a design tool: Wind loads assessment on a high-rise building. Journal of Wind Engineering and Industrial Aerodynamics, 180, 1−18. https://doi.org/10.1016/j.jweia.2018.07.009

[21] Lamberti, G., & Gorlé, C. (2020). Sensitivity of LES predictions of wind loading on a high-rise building to the inflow boundary condition. Journal of Wind Engineering and Industrial Aerodynamics, 206, 104370. https://doi.org/10.1016/j.jweia.2020.104370

[22] Zheng, X., Montazeri, H., & Blocken, B. (2020). CFD simulations of wind flow and mean surface pressure for buildings with balconies: Comparison of RANS and LES. Building and Environment, 173, 106747. https://doi.org/10.1016/j.buildenv.2020.106747

[23] Elshaer, A., Gairola, A., Adamek, K., & Bitsuamlak, G. (2017). Variations in wind load on tall buildings due to urban development. Sustainable Cities and Society, 34, 264−277. http://dx.doi.org/10.1016/j.scs.2017.06.008

[24] Nozu, T., Tamura, T., Takeshi, K., & Akira, K. (2015). Mesh-adaptive LES for wind load estimation of a high-rise building in a city. Journal of Wind Engineering and Industrial Aerodynamics, 144, 62−69. http://dx.doi.org/10.1016/j.jweia.2015.05.007

[25] Salehinejad, M. M., & Flay, R. G. J. (2021). A review of approaches to generate equivalent static and synthetic wind loads on tall buildings for the preliminary stage of design. Journal of Wind Engineering and Industrial Aerodynamics, 219, 104823. https://doi.org/10.1016/j.jweia.2021.104823

[26] Kareem, A. (1985). Lateral-torsional motion of tall buildings to wind loads. Journal of Structural Engineering, 111(11), 2479-2496. https://doi.org/10.1061/(ASCE)0733-9445(1985)111:11(2479)

[27] Kareem, A. (1992). Dynamic response of high-rise buildings to stochastic wind loads. Journal of Wind Engineering and Industrial Aerodynamics, 42(1-3), 1101-1112. https://doi.org/10.1016/0167-6105(92)90117-S

[28] Kijewski, T., & Kareem, A. (1998). Dynamic wind effects: a comparative study of provisions in codes and standards with wind tunnel data. Wind and Structures, 1(1), 77−

109. https://doi.org/10.12989/was.1998.1.1.077

[29] Swaddiwudhipong, S., & Khan, M. S. (2002). Dynamic response of wind-excited building using CFD. Journal of Sound and Vibration, 253(4), 735−754. https://doi.org/10.1006/jsvi.2000.3508

[30] Chen, X., & Kareem, A. (2005). Dynamic wind effects on buildings with 3D coupled modes: application of high frequency force balance measurements. Journal of Engineering Mechanics, 131(11), 1115−1125. https://doi.org/10.1061/(ASCE)0733-9399(2005)131:11(1115)

[31] Li, Q. S., Yang, K., Wong, C. K., & Jeary, A. P. (2003). The effect of amplitude-dependent damping on wind-induced vibrations of a super tall building. Journal of Wind Engineering and Industrial Aerodynamics, 91(9), 1175−1198. http://dx.doi.org/10.1016/S0167-6105(03)00080-1

[32] Huang, S., Li, R., & Li, Q. S. (2013). Numerical simulation on fluid-structure interaction of wind around super-tall building at high Reynolds number conditions. Structural Engineering & Mechanics, 46(2), 197−212. https://doi.org/10.12989/sem.2013.46.2.197

[33] Han, Y. D., Chun, Q., & Hua, Y. W. (2021). Wind-induced vibration of traditional Chinese citygate buildings in the Ming-Qing dynasties–A case study of the Nanjing drum tower. International Journal of Architectural Heritage, 1-20. https://doi.org/10.1080/15583058.2021.1953191

[34] Lu, X. Z., Gu, D. L., & Kareem A. (2019). Computational simulation of wind-induced motion of tall buildings in cityscapes. The 15th International Conference on Wind

Engineering (ICWE15), Beijing, China.

[35] Alemayehu, T. F., & Bitsuamlak, G. (2022). Autonomous urban topology generation for urban flow modeling. Sustainable Cities and Society, 87, 104181. https://doi.org/10.1016/j.scs.2022.104181

[36] Tseng, Y. H., Meneveau, C., & Parlange, M. B. (2006). Modeling flow around bluff bodies and predicting urban dispersion using large eddy simulation. Environmental Science & Technology, 40(8), 2653−2662. https://doi.org/10.1021/es051708m

[37] Xie, Z. T., & Castro, I. P. (2009). Large-eddy simulation for flow and dispersion in urban streets. Atmospheric Environment, 43(13), 2174−2185. https://doi.org/10.1016/j.atmosenv.2009.01.016

[38] Liu, Y. S., Cui, G. X., Wang, Z. S., & Zhang, Z. S. (2011). Large eddy simulation of wind field and pollutant dispersion in downtown Macao. Atmospheric environment, 45(17), 2849−2859. https://doi.org/10.1016/j.atmosenv.2011.03.001

[39] Letzel, M. O., Helmke, C., Ng, E., An, X., Lai, A., & Raasch, S. (2012). LES case study on pedestrian level ventilation in two neighbourhoods in Hong Kong. Meteorologische Zeitschrift, 21(6), 575−589. https://doi.org/10.1127/0941-2948/2012/0356

[40] Nakayama, H., Takemi, T., & Nagai, H. (2012). Large-eddy simulation of urban boundary-layer flows by generating turbulent inflows from mesoscale meteorological simulations. Atmospheric Science Letters, 13(3), 180−186. https://doi.org/10.1002/asl.377

[41] Gousseau, P., Blocken, B., Stathopoulos, T., & van Heijst, G. F. (2015). Near-field pollutant dispersion in an actual urban area: Analysis of the mass transport mechanism by

high-resolution Large Eddy Simulations. Computers & Fluids, 114, 151−162. https://doi.org/10.1016/j.compfluid.2015.02.018

[42] Park, S. B., Baik, J. J., & Han, B. S. (2015). Large-eddy simulation of turbulent flow in a densely built-up urban area. Environmental Fluid Mechanics, 15(2), 235−250. https://doi.org/10.1007/s10652-013-9306-3

[43] Adamek, K., Vasan, N., Elshaer, A., English, E., & Bitsuamlak, G. (2017). Pedestrian level wind assessment through city development: A study of the financial district in Toronto. Sustainable Cities and Society, 35, 178−190. https://doi.org/10.1016/j.scs.2017.06.004

[44] Jacob, J., & Sagaut, P. (2018). Wind comfort assessment by means of large eddy simulation with lattice Boltzmann method in full scale city area. Building and Environment, 139, 110−124. https://doi.org/10.1016/j.buildenv.2018.05.015

[45] Kurppa, M., Hellsten, A., Auvinen, M., Raasch, S., Vesala, T., & Järvi, L. (2018). Ventilation and air Quality in city blocks using large-eddy simulation — urban planning perspective. Atmosphere, 9(2), 65. https://doi.org/10.3390/atmos9020065

[46] Merlier, L., Jacob, J., & Sagaut, P. (2019). Lattice-Boltzmann large-eddy simulation of pollutant dispersion in complex urban environment with dense gas effect: Model evaluation and flow analysis. Building and Environment, 148, 634−652. https://doi.org/10.1016/j.buildenv.2018.11.009

[47] Auvinen, M., Boi, S., Hellsten, A., Tanhuanpää, T., & Järvi, L. (2020). Study of realistic urban boundary layer turbulence with high-resolution large-eddy simulation. Atmosphere, 11(2), 201. http://dx.doi.org/10.3390/atmos11020201

[48] Ishihara, T., Qian, G. W., & Qi, Y. H. (2020). Numerical study of turbulent flow fields in urban areas using modified $k-\varepsilon$ model and large eddy simulation. Journal of Wind Engineering and Industrial Aerodynamics, 206, 104333. https://doi.org/10.1016/j.jweia.2020.104333

[49] Gu, D. L., Zhao, P. J., Chen, W., Huang, Y. L., & Lu, X. Z. (2021). Near real-time prediction of wind-induced tree damage at a city scale: Simulation framework and case study for Tsinghua University campus. International Journal of Disaster Risk Reduction, 53, 102003. https://doi.org/10.1016/j.ijdrr.2020.102003

[50] Gu, D. L., Chen, W., & Lu, X. Z. (2022). Automated assessment of wind damage to windows of buildings at a city scale based on oblique photography, deep learning and CFD. Journal of Building Engineering, 52, 104355. https://doi.org/10.1016/j.jobe.2022.104355

[51] Kwon, D. K., Spence, S. M., & Kareem, A. (2014). A cyberbased data-enabled design framework for high-rise buildings driven by synchronously measured surface pressures. Advances in Engineering Software, 77, 13-27. https://doi.org/10.1016/j.advengsoft.2014.07.001

[52] Kwon, D. K., Spence, S. M., & Kareem, A. (2015). Performance evaluation of database-enabled design frameworks for the preliminary design of tall buildings. Journal of Structural Engineering, 141(10), 04014242. https://doi.org/10.1061/(ASCE)ST.1943-541X.0001229

[53] Lu, X. Z., McKenna, F., Cheng, Q. L., Xu, Z., Zeng, X., & Mahin, S. A. (2020). An open-source framework for regional earthquake loss estimation using the city-scale nonlinear

time history analysis. Earthquake Spectra, 36(2), 806−831. https://doi.org/10.1177/8755293019891724

[54] Lu, X. Z., & Guan, H. (2021). Earthquake Disaster Simulation of Civil Infrastructures: from Tall Buildings to Urban Areas. Springer, Singapore.

[55] Lu, X. Z., Gu, D. L., Xu, Z., Xiong, C., & Tian, Y. (2020). CIM-powered multi-hazard simulation framework covering both individual buildings and urban areas. Sustainability, 12(12), 5059. https://doi.org/10.3390/su12125059

[56] Federal Emergency Management Agency (FEMA). (2012). Multi-Hazard Loss Estimation Methodology HAZUS-MH 2.1 Advanced Engineering Building Module (AEBM) Technical and User's Manual, Tech. Rep. FEMA-P58, Washington, D.C.

[57] Xiong, C., Lu, X. Z., Hori, M., Guan, H., & Xu, Z. (2015). Building seismic response and visualization using 3D urban polygonal modeling. Automation in Construction, 55, 25−34. http://dx.doi.org/10.1016/j.autcon.2015.03.023

[58] Kwok, K. C. S., Burton, M. D., & Abdelrazaq, A. K. (2015). Wind-Induced Motion of Tall Buildings: Designing for Habitability. American Society of Civil Engineers, USA. https://doi.org/10.1061/9780784413852

[59] Setareh, M. (2010). Vibration serviceability of a building floor structure. II: Vibration evaluation and assessment. Journal of Performance of Constructed Facilities, 24(6), 508−518. https://doi.org/10.1061/(ASCE)CF.1943-5509.0000135

[60] Tamura, Y., & Kareem, A. (2013). Advanced Structural Wind Engineering (Vol. 482). Springer, New York.

[61] Ma, X. L., Xu, F. Y., Kareem, A., & Chen, T. G. (2016). Estimation of surface pressure extremes: Hybrid data and simulation-based approach. Journal of Engineering Mechanics, Volume 142, 142(10), 04016068. https://doi.org/10.1061/(ASCE)EM.1943-7889.0001127

[62] American Society of Civil Engineers (ASCE). (2011). Minimum Design Loads for Buildings and Other Structures, ASCE/SEI 7−10. ASCE, Reston, Virginia, USA.

[63] NatHaz Lab & VORTEX-Winds Group. (2022). Damping Database. http://evovw.ce.nd.edu/damping/dampingdb_noauth1.php. (accessed 6 March 2022)

[64] Jeary, A. P. (1986). Damping in tall buildings — a mechanism and a predictor. Earthquake Engineering & Structural Dynamics, 14(5), 733−750. https://doi.org/10.1002/eqe.4290140505

[65] Spence, S. M., & Kareem, A. (2014). Performance-based design and optimization of uncertain wind-excited dynamic building systems. Engineering Structures, 78, 133-144. https://doi.org/10.1016/j.engstruct.2014.07.026

[66] Kwon, D. K., & Kareem, A. (2013). A multiple database-enabled design module with embedded features of international codes and standards. International Journal of High-Rise Buildings, 2(3), 257−269. https://doi.org/10.21022/IJHRB.2013.2.3.257

[67] Architectural Institute of Japan (AIJ). (2004). Guidelines for the Evaluation of Habitability to Building Vibration. AIJ, Tokyo.

[68] International Organization for Standardization (IOS). (2007). Bases for Design of Structures — Serviceability of Buildings and Walkways Against Vibrations, ISO 10137.

1 ISO, Switzerland.